



CHORUS

This is the accepted manuscript made available via CHORUS. The article has been published as:

Unidirectional Transition Waves in Bistable Lattices

Neel Nadkarni, Andres F. Arrieta, Christopher Chong, Dennis M. Kochmann, and Chiara Daraio

Phys. Rev. Lett. **116**, 244501 — Published 13 June 2016

DOI: [10.1103/PhysRevLett.116.244501](https://doi.org/10.1103/PhysRevLett.116.244501)

Unidirectional Transition Waves in Bistable Lattices

Neel Nadkarni¹, Andres F. Arrieta^{2,3}, Christopher Chong^{3,4}, Dennis M. Kochmann¹, Chiara Daraio^{1,3}

¹*Graduate Aerospace Laboratories, California Institute of Technology, Pasadena, California 91125, USA*

²*School of Mechanical Engineering, Purdue University, West Lafayette, Indiana 47905, U.S.A*

³*Department of Mechanical and Processing Engineering, ETH Zurich, Zurich CH-8092 Switzerland and*

⁴*Department of Mathematics, Bowdoin College, Brunswick, Maine 04011, USA*

We present a model system for strongly nonlinear transition waves generated in a periodic lattice of bistable members connected by magnetic links. The asymmetry of the on-site energy wells created by the bistable members produces a mechanical diode that supports only unidirectional transition wave propagation with constant wave velocity. We theoretically justify the cause of the unidirectionality of the transition wave and confirm these predictions by experiments and simulations. We further identify how the wave velocity and profile are uniquely linked to the double-well energy landscape, which serves as a blueprint for transition wave control.

Introduction.— Unidirectional wave-guiding is a rare phenomenon of interest for mechanical diodes, rectifiers or switches that propagate stress waves in designated directions but not in reverse. For acoustic waves, this has been achieved through carefully engineered periodic lattices and topological metamaterials that exploit time-reversal asymmetry or transmission asymmetry, see e.g. [1–7]. Such systems, providing one-way acoustic insulation, are typically studied in the linearized regime and the associated elastic pressure waves display small amplitudes (and quickly decay in realistic structures with internal damping). **In weakly-nonlinear lattices, directional wave-guiding has been achieved using cubic Kerr nonlinearities in non-homogenous systems** [8, 9]. However, strongly-nonlinear directional wave guides for the transmission of finite amplitude pulses or the mitigation of impact shock waves have remained largely unexplored, partly due to their mathematical complexity and limited experimental realizations. Only one macroscopic experiment that has verified stable nonlinear transition waves in a chain of elastically-coupled rotational pendula [10]; and that system was bidirectional. Here, we present an instructive **homogenous** mechanical model that displays tunable unidirectional guiding of strongly-nonlinear transition waves and admits theoretical insight that agrees well with experimental findings.

Transition waves are commonly found in systems which permit switching between multiple stable equilibria (the energetic characteristics of which will be key to controllable unidirectionality). These play a central role in a multitude of mechanical phenomena such as dislocation motion in crystals [11], ferroelectric phase transitions [12], structural collapse [13], transitions due to shape memory effect [14], transformational plasticity [15] and nanoscale structural mechanics [16]. Phase transition scenarios in which the effects of lattice dispersion are balanced by the nonlinear medium have been investigated theoretically, see, e.g., [17–24] and references therein. Unfortunately, the lack of accessible experimental systems has left many previous theoretical studies unchallenged and, as a consequence, has rendered mechan-

ical diodes in the nonlinear regime a rare find.

In this Letter, we identify stable unidirectional transition wave propagation theoretically and experimentally in a 1D periodic lattice or “meta-structure” of bistable mechanical elements connected by nonlinear links. The double-well on-site potential is realized by pre-stressed composite shells which snap elastically from one stable equilibrium to another while undergoing large, nonlinear deformation. Magnetic inter-element connections generate nonlinear repulsive forces between bistable lattice members. As we demonstrate theoretically and verify numerically, the asymmetric potential energy wells make the wave propagation unidirectional: the transition from high to low energy produces a stable transition wave, whereas the reverse transition from low to high energy disintegrates incoming pressure waves, thereby acting as a diode for large-amplitude waves. This is in line with our general theoretical observations [25]. This unidirectionality has potential for wave mitigation, impact energy absorption applications, or mechanical switches and filters. The described experimental setup serves as a model system that can enable the investigation of the rich nonlinear dynamics of periodic arrays with, in principle, arbitrary multi-stable on-site energy topologies.

Experimental system.— The experimental setup consists of an array of bistable composite shells with an inter-element magnetic forcing. Individual bistable elements are made from carbon fiber reinforced plastic prepregs, laminated with a precise spatially distributed arrangement of laminae in the 0° and 90° directions. (see geometry and manufacturing details in *Supplemental Material* [26]). The combination of microstructure and cooldown after curing at elevated temperature induces a particular deformation field producing composite laminates exhibiting a tailorable strain potential topology, while admitting clamping of two opposite edges [27]. The strain energy stored in the bistable laminate as a function of the out-of-plane displacement can be further tailored by varying the clamping distance, as well as the fiber distribution [28]. The topology of the resulting potential is inherently asymmetric with one of the

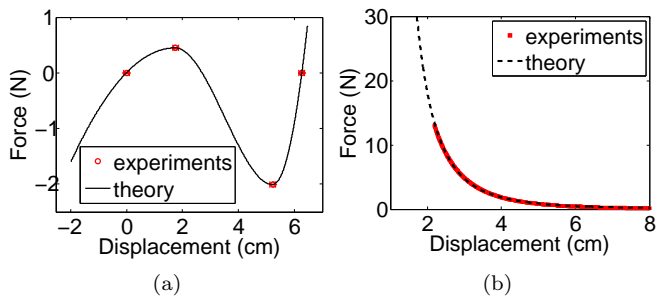
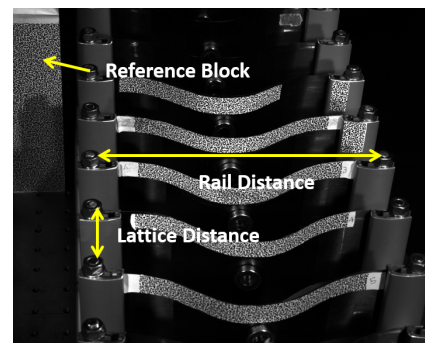


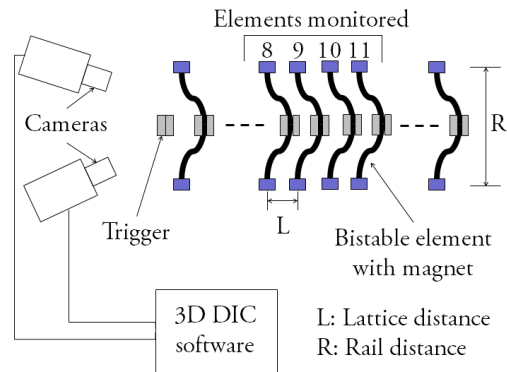
Figure 1. (a) Force displacement curve of the bistable element for clamping distance of 21.5 cm. The critical snapping points (maximum force) and equilibrium points are identified and fitted with splines while maintaining continuity in stiffness. (b) Magnetic force vs displacement plot for an NSNS-SNSN configuration. Numerical fit: $F = Ad^p$ with $A = 4.95e-05$ N/m p and $p = -3.274$.

wells having a lower energy than the other. To model the bistable element, the force-displacement curve is obtained with quasi-static displacement controlled tests which is fit with splines, see Fig. 1(a). The magnitude of the snapping force is much higher at one transition point than the other. Furthermore, desired levels of force-displacement asymmetry and transition values can be designed by modifying the fiber distribution of the used bistable members as required to control the characteristics of the propagating transition waves. The lattice used for experimentation consists of 20 bistable elements which are supported using clamps mounted on an aluminum rail. The rails are fixed to an optical table. Each bistable element is fitted on either face with two NdFeB ring magnets. Similar to [29], the force displacement curve of the magnets, shown in Fig. 1(b), is fitted using a best fit relation of the form: $F = Ad^p$ where F is the force and d is the displacement. The magnets are fixed to the bistable laminates and are arranged in a NSNS-SNSN configuration to exert repelling forces between the elements. They are laser aligned so that all lie along a straight line. A stereoscopic digital image correlation system with a rate of 4000 fps is used to acquire the displacements of four consecutive representative bistable elements. The initial displacement is triggered using a precision screw which provides a repeatable perturbation to the first lattice element. The lattice used for experimentation is shown in Fig. 2.

Stable wave propagation.— We study the transition from the high energy well to the lower energy well. All the bistable elements in the system are placed in the high energy well and the first element is forced to snap to the lower energy state. The rail distance R is defined as the distance between the clamps at the two ends of the bistable element and the lattice distance L is the distance between two elements in the chain. We present results for three representative cases of stable wave propagation



(a)



(b)

Figure 2. (a) The experimental lattice is shown along with the trigger magnet mounted on a precision screw. The displacements of elements 8 to 11 that are marked using a speckle pattern are tracked using a digital image correlation software (DIC). (b) A schematic of the experimental measurement technique is shown. The two cameras are synchronized and capture the 3D deformation field of the tracked specimens. The out-of-plane deformation is obtained using the Vic-3D DIC software.

in Fig. 3 for various choices of R and L . Each experiment was repeated three times to obtain statistical variations. In general, the results obtained were highly repeatable. The deformation of the bistable element is 3D in nature; however, the out-of-plane displacement is significantly higher than the in-plane deformation, thereby causing the wave propagation to be quasi-1D, as can be observed in the snap-shot sequence of the propagating wave in the *Supplemental Materials* [26]. Experiments are compared with numerical simulations of the following 1D model of the discrete lattice:

$$mu u_{n,tt} + A(u_{n+1} - u_n + L)^p - A(u_n - u_{n-1} + L)^p + \alpha u_{n,t} + \beta \phi'(u_n) = 0, \quad (1)$$

where u_n is the displacement of the n th particle from its static equilibrium, A and $p < -1$ are parameters of the inter-element forcing function, m is the mass of the four magnets that compose each connecting element, L is the lattice distance, $\alpha > 0$ is the dissipation constant and $\beta \phi(u)$ is a bistable potential where β is a constant. The

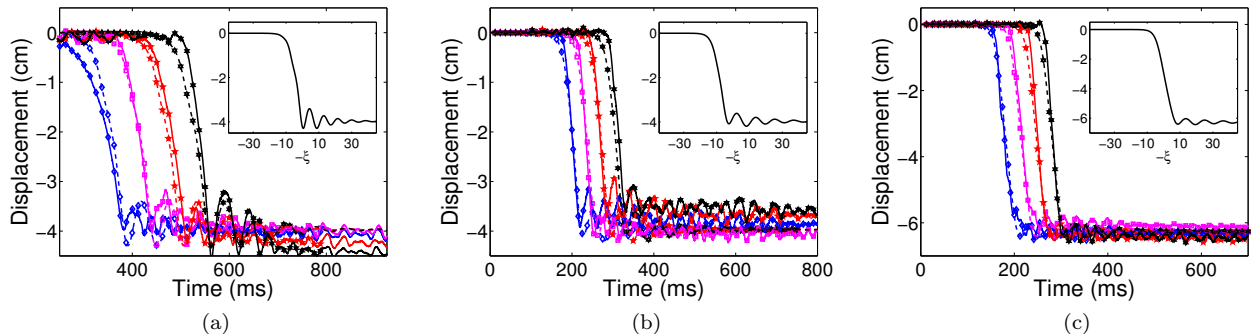


Figure 3. (a), (b) & (c) Transition wave propagation for three different combinations of lattice distance (L) and rail distance (R). The displacement time series is shown for the 8th - 11th element (blue diamonds, magenta squares, red 5 point stars and black 6 point stars respectively) for (a) $L = 8$ cm, $R = 22.5$ cm (b) $L = 6$ cm, $R = 22$ cm and (c) $L = 8$ cm, $R = 21.5$ cm. The negative values of the displacements indicate that the elements are deforming away from the camera. The direct numerical simulations of the discrete particle model Eq. (1) (dashed lines) are in good agreement with the experimental results (solid lines). The inset of each panel is the numerical solution of Eq. 14 of the *Supplemental Materials* [26], which corresponds to an exact transition wave. On reaching the boundary, the waves do not reflect back into the bulk and hence the transition is unidirectional. Refer to the *Supplemental Materials* [26] for the snapshot sequence, and video showing unidirectional stable wave propagation, i.e., waves propagate in one direction and not in the opposite direction.

parameters A, p and the bistable potential $\beta\phi(u)$ are determined through the fitting procedure described above. Indices following a comma denote differentiation. The simulations are performed using a Newmark time integration scheme [30]. We expect the dissipation parameter to depend on the snapping trajectory of an individual bistable element, which is linked only to the rail distance. Therefore we assume α to be independent of the lattice distance and to only depend on the rail distance. For each rail distance R , the dissipation parameter α is calculated by matching the numerically obtained wave velocity with experiments for a fixed value of the lattice distance L . The snapping equilibrium distances for the used elements is slightly different ($\sim \pm 10\%$) owing to variability induced during the composite manufacturing process. Nevertheless, this variation does not affect the underlying physical behavior under examination. Comparing Figs. 3(a) and 3(b), we see that the strain of the wave transition profile is broader for larger lattice spacings (Fig. 3(a)) and more spatially localized for small lattice spacings (Fig. 3(b)). The variation of wave localization (i.e. width of strain profile) and velocity as functions of lattice distance for different rail distances are shown in Fig. 4. The experimental result for $R = 21.5$ cm and $L = 6$ cm is an outlier in Fig. 4(a). This is due to the fact that L (6 cm) is smaller than the snapping distance (~ 6.2 cm). This causes multiple intermediate snaps during the transition of the bistable element and the quasi-1D approximation fails to hold, thereby causing the experimental data to significantly deviate from the numerical results. The control parameters L and R allow for designing the level of wave localization as shown in Fig. 4(b). Interestingly, in the proposed sys-

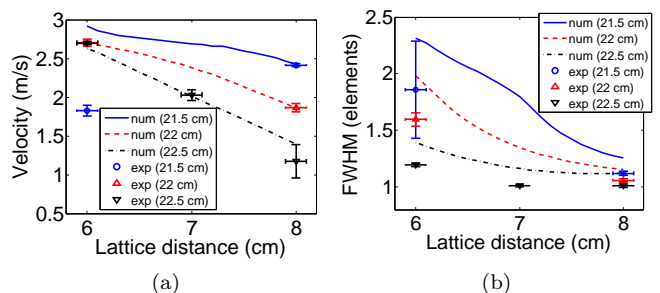


Figure 4. (a) Wave velocity as a function of lattice distance for different rail distances. The dissipation parameter has been optimized such that the wave velocity matches for lattice distance 8 cm for rail distances 21.5 cm and 22 cm, and lattice distance 7 cm for rail distance 22.5 cm. (b) Full width at half maximum (FWHM) of the strain profile of the transition wave as a function of lattice distance for different rail distances.

tem, transition waves can be localized almost on a single element allowing for tightly packed and remarkably stable energy transmission. Hence, the waves can be localized to a single particle, similar to the case of repelling magnet chains [29]. This compares with a minimum of approximately 2.2 particles for pressure waves in granular chains [31, 32].

An interesting observation is that the steady state wave velocity appears to be independent of the initial excitation condition. For example, stronger initial impacts do not lead to faster waves, which is in contrast to the case of the granular chain [32]. Indeed, it appears the combination of an asymmetric bistable potential and the presence of damping leads to unique wave velocities, making this system more akin to reaction diffusion type equations [33]

rather than Hamiltonian lattices such as those of the Klein-Gordon type [34, 35] (e.g. the Frenkel-Kontorova equation [11]) and Fermi-Pasta-Ulam type [36, 37] (e.g. the granular chain [32]). To probe this point even further, we restrict our attention to traveling wave solutions of the form of Eq. (1), namely those of the form $u_n(t) = u(Ln - vt) = u(\xi)$, where $u(\xi), \xi \in \mathbb{R}$ satisfies the advance-delay differential equation

$$v^2 m u_{\xi\xi} - v \alpha u_{\xi} + \beta \phi'(u) + A(u(\xi + L) - u(\xi) + L)^p - A(u(\xi) - u(\xi - L) + L)^p = 0. \quad (2)$$

We found that despite varying the initial guess for solving Eq. (2) numerically, our algorithm converges to the same profile and wave velocity v , implying that for a fixed set of system parameters, there is a unique wave velocity of the transition wave. The traveling wave formulation (2) is also natural for bifurcation and sensitivity studies. For example, the variation of the wave velocity with respect to the interaction potential coefficient p , and level of asymmetry are presented in the *Supplemental Material* [26].

Wave disintegration.— Advance-delay differential equations such as Eq. (2) are notoriously difficult to analyze. One can obtain a system that is analytically tractable by considering the limit of small lattice spacing. In the case of Eq. (1), this results in the fourth order ordinary differential equation (see *Supplemental Material* [26] for derivation),

$$-\frac{1}{24} a^2 \rho c_0^2 [(p-2)(p-1)u_{\xi\xi}^3(u_{\xi} + 1)^{p-3} + 4(p-1)u_{\xi\xi}u_{\xi\xi\xi}(u_{\xi} + 1)^{p-2} + 2u_{\xi\xi\xi\xi}(u_{\xi} + 1)^{p-1}] \quad (3) \\ \rho v^2 u_{\xi\xi} - \rho c_0^2 u_{\xi\xi}(1 + u_{\xi})^{p-1} - v\gamma u_{\xi} + \psi'(u) = 0,$$

with $\xi = nL - vt$, $\rho = m/L$, $\rho c_0^2 = -AL^p p$, $\gamma = \alpha/L$, $\beta \phi'(u_n)/L = \psi'(u_n)$ and the subscript ξ implies differentiation. It can be shown that for stable wave propagation (see *Supplemental Material* for derivation),

$$\psi(u_i) - \psi(u_f) = v\gamma \int_{-\infty}^{\infty} u_{\xi}^2 d\xi \geq 0 \Rightarrow \psi(u_i) \geq \psi(u_f). \quad (4)$$

Eq. (4) shows that the final state cannot have a higher energy than the initial state for stable wave propagation. This is because, in the case of high-to-low energy transition, the release of stored potential energy counters the effect of dissipation. This is not possible for a low-to-high energy transition. Therefore, in the case of an asymmetric bistable potential, a transition is allowed from the higher energy state to a lower energy state, as seen in the previous experiments; however in the opposite case, the wave does not propagate. The problem can also be approached through the entropy relation for phase boundary propagation [23]. Identifying

that $\Delta\psi = \psi(u(\xi \rightarrow \infty)) - \psi(u(\xi \rightarrow -\infty))$ is the driving force on the transition wave, (4) can be rewritten as the entropy inequality,

$$v\Delta\psi \geq 0. \quad (5)$$

Hence, the entropy inequality implicitly gives rise to the condition for unidirectional stable wave propagation in the discrete lattice. We observe this phenomenon in experiments. When all the elements are placed in the low energy well and a transition is forced, the elements snap back to their original low energy state. In addition, the video in the *Supplemental Material* [26] shows this effect. Therefore, the lattice works as a nonlinear unidirectional waveguide for transition waves.

Theoretical estimates of wave characteristics.— Using (4), the average kinetic energy transported ($\langle E \rangle$) can be computed as

$$\langle E \rangle = \frac{\Delta\psi}{2\gamma} \rho v \quad (6)$$

(with $\rho = m/L$) which scales linearly with the velocity of wave propagation [25]. The governing equation (3) also provides bounds for maximum particle velocity. When the particle velocity $u_t = -vu_{\xi}$ attains a maximum, the acceleration $u_{tt} = v^2 u_{\xi\xi} = 0$ is zero. Substituting this in (3) gives

$$|\frac{1}{12} a^2 c_0^2 u_{\xi\xi\xi\xi}^* (-A/v + 1)^{p-1}| = |-\gamma A + \psi'(u^*)|, \quad (7)$$

where the * superscript indicates evaluation where u_{ξ} is at a maximum. In the continuum limit ($a \rightarrow 0$), the term on the left hand side in (7) is very small. Therefore,

$$A \simeq \psi'(u^*)/\gamma \leq F_m/\gamma \quad (8)$$

where F_m is the maximum force or the snapping force of the bistable element and u^* is the displacement at maximum u_{ξ} , thus providing an upper bound estimate of the maximum particle velocity. The width of the strain profile of the transition wave can be estimated by assuming an ansatz of the form,

$$u_{\xi}(\xi) = \frac{A}{v} \operatorname{sech}^2 \frac{1.76 \xi}{w} \quad (9)$$

where the w is the full width at half maximum (FWHM). Substituting (9) in (4) and evaluating the integral yields

$$w = 1.32 \frac{v\Delta\psi}{A^2\gamma} \geq 1.32 \frac{\gamma v\Delta\psi}{F_m^2}, \quad (10)$$

thus providing a lower bound on the width of the wave (or the amount of localization that can be achieved).

Conclusions.— We have introduced a model lattice system comprised of tailored bistable elements connected by magnets sustaining strongly nonlinear unidirectional propagation of transition pressure waves. A reduced 1D

discrete analytical model is developed which allows for wave tailoring, by designing the strain potential topology of the bistable members, the direction of propagation, velocity and profile of the transition waves. The designed on-site potential exhibited by the bistable members enables the realization of mechanical diodes and wave guides with far-reaching applications, from energy absorption and harvesting, to impact mitigation and imaging. In addition, our model system allows for accessible experimental investigation of hitherto difficult to access transition wave phenomena in solids.

Acknowledgements.— The authors are thankful for discussions with P.G. Kevrekidis. N.N. and C.D. gratefully acknowledge financial support from the National Science Foundation (NSF) under grant CMMI-1200319. The work of C.C. was partially supported by the ETH Zurich Foundation through the Seed Project ESC-A 06-14. The authors thank P. Ermanni for providing access to his experimental facilities and equipment; the DIC system was acquired thanks to the SNF R’Equip grant n. 206021.150729 and the complementary ETH Scientific Equipment Programme. D.M.K. acknowledges support from NSF through CAREER award CMMI-1254424. N.N. and A.F.A. would like to thank Giulio Molinari and Jean-Claude Tomasina for assistance in setting up the experiments.

-
- [1] B.-I. Popa and S. A. Cummer, *Nature Communications* **5** (2014).
- [2] R. Krishnan, S. Shirota, Y. Tanaka, and N. Nishiguchi, *Solid State Communications* **144**, 194 (2007).
- [3] X. Zhu, X. Zou, B. Liang, and J. Cheng, *Journal of Applied Physics* **108**, 124909 (2010).
- [4] X.-F. Li, X. Ni, L. Feng, M.-H. Lu, C. He, and Y.-F. Chen, *Physical Review Letters* **106**, 084301 (2011).
- [5] N. Boechler, G. Theocharis, and C. Daraio, *Nature Materials* **10**, 665 (2011).
- [6] B. Liang, X. Guo, J. Tu, D. Zhang, and J. Cheng, *Nature Materials* **9**, 989 (2010).
- [7] M. Ruzzene, F. Scarpa, and F. Soranna, *Smart Materials and Structures* **12**, 363 (2003).
- [8] M. Scalora, J. P. Dowling, C. M. Bowden, and M. J. Bloemer, *Journal of Applied Physics* **76** (1994).
- [9] N.-S. Zhao, H. Zhou, Q. Guo, W. Hu, X.-B. Yang, S. Lan, and X.-S. Lin, *JOSA B* **23**, 2434 (2006).
- [10] A. C. Scott, *American Journal of Physics* **37**, 52 (1969).
- [11] Y. Frenkel and T. Kontorova, *Phys. Z. Sowjetunion* **13**, 1 (1938).
- [12] P. Giri, K. Choudhary, A. Dey, A. Biswas, A. Ghosal, and A. K. Bandyopadhyay, *Phys. Rev. B* **86**, 184101 (2012).
- [13] A. Cherkaev, E. Cherkaev, and L. Slepyan, *Journal of the Mechanics and Physics of Solids* **53**, 383 (2005).
- [14] F. Falk, *Zeitschrift für Physik B Condensed Matter* **54**, 159 (1984).
- [15] L. Truskinovsky and A. Vainchtein, *Journal of the Mechanics and Physics of Solids* **52**, 1421 (2004).
- [16] I. Benichou and S. Givli, *Phys. Rev. Lett.* **114**, 095504 (2015).
- [17] N. Nadkarni, C. Daraio, and D. M. Kochmann, *Phys. Rev. E* **90**, 023204 (2014).
- [18] J. C. Comte, P. Marquie, and M. Remoissenet, *Phys. Rev. E* **60**, 7484 (1999).
- [19] A. M. Balk, A. V. Cherkaev, and L. I. Slepyan, *J. Mech. Phys. Solids* **49**, 149 (2001).
- [20] L. Truskinovsky and A. Vainchtein, *SIAM Journal on Applied Mathematics* **66**, 533 (2005).
- [21] O. M. Braun, Y. S. Kivshar, and I. I. Zelenskaya, *Phys. Rev. B* **41**, 7118 (1990).
- [22] O. M. Braun and Y. S. Kivshar, *Physics Reports* **306**, 1 (1998).
- [23] R. Abeyaratne and J. Knowles, *Archive for Rational Mechanics and Analysis* **114**, 119 (1991).
- [24] M. Remoissenet and M. Peyrard, *Physical Review B* **29**, 3153 (1984).
- [25] N. Nadkarni, C. Daraio, R. Abeyaratne, and D. M. Kochmann, *Phys. Rev. B* **93**, 104109 (2016).
- [26] See Supplemental Material at http://to_be_provided which includes [38–40], for theoretical derivations, composite manufacturing and experimental details.
- [27] A. F. Arrieta, I. K. Kuder, T. Waeber, and P. Ermanni, *Composites Science and Technology* **97**, 12 (2014).
- [28] I. K. Kuder, A. F. Arrieta, and P. Ermanni, *Composite Structures* **122**, 445 (2015).
- [29] M. Molerón, A. Leonard, and C. Daraio, *Journal of Applied Physics* **115**, 184901 (2014).
- [30] N. M. Newmark, *Journal of the Engineering Mechanics Division* **85**, 67 (1959).
- [31] V. F. Nesterenko, *Appl. Mech. Tech. Phys.* **24**, 733 (1984).
- [32] V. Nesterenko, *Dynamics of Heterogeneous Materials* (Springer-Verlag New York, 2001).
- [33] J. Xin, *SIAM Review* **42**, 161 (2000).
- [34] Y. Zolotaryuk, in *Nonlinear Waves: Classical and Quantum Aspects*, NATO Science Series II: Mathematics, Physics and Chemistry, Vol. 153, edited by F. Abdullaev and V. Konotop (Springer Netherlands, 2005) pp. 521–528.
- [35] G. Iooss and K. Kirchgässner, *Communications in Mathematical Physics* **211**, 439 (2000).
- [36] G. Friesecke and J. A. D. Wattis, *Comm. Math. Phys.* **161**, 391 (1994).
- [37] G. Iooss, *Nonlinearity* **13**, 849 (2000).
- [38] I. K. Kuder, A. F. Arrieta, and P. Ermanni, *Composite Structures* **122**, 445 (2015).
- [39] H. Xu, P. Kevrekidis, and A. Stefanov, *Journal of Physics A: Mathematical and Theoretical* **48**, 195204 (2015).
- [40] T. Erneux and G. Nicolis, *Physica D: Nonlinear Phenomena* **67**, 237 (1993).